Spectral Analysis of Bulk Reflectance from Coastal Waters: Deconvolution of Diffuse Spectra Due to Scattering and Absorption by Coastal Water

M. Sydor†‡, B.D. Wolz†, and A.M. Thralow†

†Department of Physics
University of Minnesota
  Duluth
Duluth, MN 55812, U.S.A.

‡Naval Research Laboratory
Code 7212
Remote Sensing Branch
Washington, DC 20375,
  U.S.A.

ABSTRACT ∎

SYDOR, M.; WOLZ B.D., and THRALOW, A.M., 2002. Spectral analysis of bulk reflectance from coastal waters: deconvolution of diffuse spectra due to scattering and absorption by coastal water. *Journal of Coastal Research*, 18(2), 352–361. West Palm Beach (Florida), ISSN 0749-0208.

We apply routine techniques of diffuse reflectance spectroscopy to establish a systematic procedure for global analysis of the *in situ* reflectance from coastal water over the 400–900 nm region of the spectrum. Our technique relies on a sequential multi-parameter fit to the reflectance in the 750–900, ~600, ~400, and ~676 nm wavelength regions of the spectrum where the bulk reflectance from coastal water can be linked to the inherent optical properties of its main constituents: pure water, inorganic suspended solids, dissolved organic matter, and phytoplankton pigment. Using *in situ* reflectance *alone*, we are able to estimate the volume scattering coefficient from suspended particles and determine the volume absorption coefficients due to inorganic particles, dissolved organic matter, and phytoplankton pigment. The predicted results for the total absorption and scattering agree within 15% of the measured values for the Mississippi Sound, Lake Superior, and Great Bay, New Jersey.

ADDITIONAL INDEX WORDS: *Ocean optics, remote sensing, diffuse reflectance spectra, volume absorption coefficient, volume scattering coefficient.*

INTRODUCTION

Analysis of the reflectance spectra from coastal regions has important practical application in the determination of nutrients, sedimentation, and biological productivity. We avoid the ill-defined empirical corrections for rough-water surface reflectance by examining the *in situ* reflectance just below the water surface (R_{RSW}). The above-surface reflectance (R_{SR}) and R_{RSW} are related through Fresnel reflectance and the index of refraction for air-water interface (see for example WHITLOCK *et al.*, 1981; JEROME *et al.*, 1996). Thus, one can extend the results for R_{RSW} to R_{SR}. The *in situ* or bulk reflectance of ocean water at any wavelength λ is defined according to: $R_{RSW} = L_u/E_d^-$ where L_u is the upwelling radiance just below the water surface and E_d^- is the downwelling irradiance just below the water surface. R_{RSW} has a diffuse character. Its rather featureless spectral shape depends on several spectrally broad optical parameters that make deconvolution of R_{RSW} into constituent spectra due to organic pigment, inorganic particles, and dissolved organic material (DOM) very difficult.

In general, R_{RSW} depends on the absorption by pure water a_w, which is relatively flat in the visible region of the spectrum, and two exponential absorption coefficients, a_{DOM}, and a_p due to DOM and inorganic particles respectively. R_{RSW} also depends on a_c, the absorption by phytoplankton pigment, gen-

erally referred to at 676 nm as chlorophyll. The spectral shape of a_c is highly variable and is usually unknown. Secondly, there are four back scattering coefficients contributing to R_{RSW}, one from each of the above constituents. Thirdly, the magnitudes of the absorption and scattering coefficients vary with the concentration of DOM, chlorophyll, and suspended solids. Finally, R_{RSW} also depends on the angular distribution of the illuminating light field (MOREL *et al.*, 1995; JEROME *et al.*, 1996). As a result, our ability to resolve R_{RSW} into constituent spectra depends largely on a careful restriction of the optical parameters used in simulation of R_{RSW}, and our ability to identify the regions of the R_{RSW} spectrum where single unknown parameters dominate its spectral shape.

The difficulty encountered in an unrestricted iterative fit to R_{RSW} can be demonstrated by using the results of JEROME *et al.* (1996). The authors show that R_{RSW} depends only on b_b/a, the ratio of the volume back scattering coefficient to the total volume absorption coefficient. Clearly, any given b_b/a can be obtained for a multiple common to b_b and a. As a result, R_{RSW} can be approximated by more than one set of parameters in the visible region of the spectrum where both a and b_b are complex and unknown. We will illustrate this problem using an example which shows that random iterative fits of R_{RSW} usually fail because in a random fit one can optimize any given parameter, say b_b, and then find an a that gives the desired b_b/a. Common oceanographic analyses of R_{RSW} that rely on band-ratios in the visible spectrum suffer from the

same ambiguity. Thus, there is a pressing need for a systematic globally valid procedure for spectral analysis of coastal water.

We accomplish a globally valid analysis by exploiting the dependence of R_{RSW} on b_b/a. However, instead of confining our analysis to the visible spectrum where a depends on many variables, we utilize the near infrared region of the spectrum from 760–900 nm (near IR), where R_{RSW} depends only on the volume scattering coefficient and the known a_w.

We first correlate R_{RSW} with the total scattering coefficient (b) in the 750–900 nm range of the spectrum to find the proportionality coefficient (C_b) in $R_{RSW} \approx C_b(b/a_w)$. This is done for variety of coastal waters. We also present experimental results showing that b has a predominate $\sim 1/\lambda$ spectral dependence (WHITLOCK et al., 1981; SYDOR et al., 1998). We assume that average C_b holds globally over the entire spectrum. Using these assumptions we can obtain from near IR an estimate of the product $C_b b$ and b from plots of R_{RSW} vs. $1/(\lambda a_w)$ for an unknown station. Subsequently, we can extend $C_b b$ to the visible region of the spectrum and simulate R_{RSW} in the visible by exploiting the exponential character of the absorption coefficients a_p and a_{DOM}. Ultimately, this procedure leaves us with one unknown, the absorption coefficient a_c. The spectral dependence of a_c is unpredictable from one geographic area to another. However, a_c has a unique chlorophyll signature at 676 nm. By using a surrogate "average" a_c that displays the prominent chlorophyll signature at 676 nm we can adjust the magnitude of the simulated R_{RSW} at 676 nm until it matches the measured R_{RSW} at 676 nm. This last step gives us an estimate the value of a_c at 676 nm. Subsequently, we set $a_c = 0$ and use a subtraction technique to establish its value at other wavelengths.

BACKGROUND

To formulate the problem mathematically, we examine the most frequently used expression for R_{RSW}. The relationship between reflectance, scattering, and absorption for ocean water was found first by using Monte Carlo solutions of the Radiative Transfer Equation by GORDON et al. (1975), and by MOREL and PRIEUR (1977). The Monte Carlo solution yields a concise approximation between the reflectance, back scattering, and the absorption, but it does not distinguish the contributions to the absorption and scattering from individual constituents. Instead, it relates R_{RSW} to total a, and b_b. If the illuminating light field has an angular distribution, as does daylight, the mathematical form for R_{RSW} at any λ can be written as:

$$R_{RSW} \cong Cb_b/(a + b_b) \quad (\text{sr}^{-1}) \qquad (1a)$$

where C is treated as a constant. In reality, C depends on Q, the ratio of the back-scattered radiance to the back-scattered irradiance (MOREL et al., 1995). C also contains an empirical factor $f \sim 0.33$ that adjusts the amplitude of the Monte Carlo solution to the observed average reflectance from ocean waters. For $b_b \gg a$, a generally valid approximation for coastal waters, equation 1 can be expanded in a binomial series giving: $R_{RSW} \cong C(b_b/a)(1 + b_b/a)^{-1} \sim C(b_b/a)(1 - b_b/a + \ldots)$. Since C is not truly a constant, JEROME et al. (1996) were

able to produce a very close polynomial fit to R_{RSW} using powers of Bb/a:

$$R_{RSW} \cong -0.00042 + 0.112(Bb/a) - 0.0455(Bb/a)^2 \quad (\text{Sr}^{-1})$$
$$\qquad (1b)$$

where $B = b_b/b$ ranged from 0.013 to 0.044. Importantly, the single polynomial given by equation 1b held for the entire range of b_b/b together with the assumption that b_b had the same spectral dependence as b. Different values of B were used by JEROME et al. (1996) to distinguish various types of water, near-shore water, open-ocean, etc. The result given by equation 1b and its assumption that b_b has the spectral dependence of b is very significant and will be used later to support our experimental relation $R_{RSW} \approx C_b b/a$.

In general, for wavelengths $400 < \lambda < 760$ nm, the right hand side of equation 1a depends on at least nine parameters. Some parameters are very difficult to measure. For instance, b_b is small compared with b, thus any stray light or vignetting overwhelms the measurement of b_b. Furthermore, measurement of b_b depends on instrument configuration i.e. it is subject to the observational geometry that changes with absorption. As yet, there is no standard instrumentation for the measurement of b_b. Similarly, mathematical characterization of a_c is also problematic because its spectral shape can vary depending on temperature, water clarity, and the concentration of nutrients.

Fortunately, some optical properties of coastal waters are predictable and allow us to write equation 1a in a more tractable form (SYDOR et al., 1998).

In coastal waters Rayleigh scattering from pure water and DOM is negligible, thus we can assume that scattering comes mainly from the suspended solids. Furthermore, suspended solids in coastal waters have small b_b/b, roughly ~ 0.02. In addition we will show that in coastal waters b_b is roughly ten times smaller than a_p. The last two conditions allow us to drop the dependence on b_b in the denominator of equation 1a when we are dealing with coastal waters. However, our most important simplification of the problem comes from the seemingly unorthodox use of b in place of b_b.

We observed that b_b for coastal waters has $\sim 1/\lambda$ behavior that is very similar to the spectral dependence of b. This is borne out by WHITLOCK et al. (1981). WHITLOCK et al. also questioned the presumed dependence of R_{SR} on b_b/a in coastal waters. Thus, in our studies of R_{SR} as a function of a and b (SYDOR et al., 1998), we considered $R_{SR} \propto b/a$ rather than b_b/a. In essence, we determined the magnitude of a new proportionality constant in place of C in equation 1a. This procedure appeared to hold for coastal waters and simplified the problem considerably. Unlike b_b, measurement of b is routine. It is performed using optical absorption and extinction (c) measurements with instruments commonly referred to as ac9 meters. The measurement of b using ac9 meters is reasonably accurate and independent of the observation angle. In summary, the above results lead us to an approximation for R_{RSW} according to:

$$R_{RSW} \approx C_b b/(a_{DOM} + a_p + a_c + a_w) \quad (\text{sr}^{-1}) \qquad (2)$$

In equation 2, we take $C_b \approx 0.0023$ as an experimental constant rather than treating it as Cb_b/b, thus equation 2 is an

experimental relation. However, we can make a simple physical argument why equation 2 is inherently sound. To do so, we use the results of JEROME et al. (1996).

It is noteworthy to point out that JEROME et al. (1996) were able to fit R_{RSW} with an accuracy of about 9% using one polynomial expression for all values of (b_b/b) ranging from 0.013 to 0.044. According to equation 2, JEROME's result implies that we would need six equations with values of C_b ranging from 0.0015 to 0.005 to describe the various types of coastal water, i.e. to describe R_{RSW} globally. In essence, we would need a separate equation for each coastal region. Yet VOLTEN et al. (1998) show that their normalized scattering function for silt off the coast of the Netherlands matches the scattering function for the San Diego Harbor, presumably because of the preponderance of inorganic particles in the near-shore waters. KIRK (1994) makes a similar assessment. To resolve these seemingly contradictory and rather fortuitous outcomes, we propose the following explanation.

In Remote Sensing and in situ measurements of the reflectance we always view a depth of water determined by the mean free absorption length of a photon $\sim 1/a$. Thus, if the mean free scattering length $\sim 1/b$ is shorter than $1/a$, we observe multiple scattering on the order of $\sim b/a$. The median value of b/a in JEROME's et al. (1996) ranges from 11 to 37 for values of $b_b/b = 0.044$ and 0.013 respectively. On the average this represents 11 to 37 collisions, at least in the visible spectrum.

Let us consider R_{RSW} for a plane wave at Normal incidence to the surface. Suppose that upon the entry into the water the angular distribution of the light field did not change as the result of scattering, i.e. the geometric factor was fixed. Then, for multiple scattering R_{RSW} should be directly proportional to the average number of scatters $\sim b/a$ times b_b/b the probability that for each scatter a fraction b_b/b of photons is scattered in the backward direction. In that case, one would indeed need a separate equation for each type of water i.e. for each b_b/b. However JEROME et al. (1996) show that all water types follow the same relationship within 9%. This result points to a simple explanation.

In reality the distribution of the light field spreads with scattering. Thus, R_{RSW} still depends on the number of collisions b/a, as above, but the angular probability that a photon heads for the detector after n collisions depends on the effective $B' = b_b'/b$ due to several collisions. One can think of B' in two equivalent ways. 1) If we track a single photon for several collisions, the probability that it heads for the detector is given by an effective phase function broadened by several collisions. 2) Alternatively, if we take the fact that the angular probability of scattering is the same for any given collision, then the probability that a photon heads for the detector after the nth collision depends on the angle it had acquired relative to the detector before the nth collision. In essence, the probability that a photon is detected after n collisions depends the single scattering phase function but sampled over angles that are not limited to $\pi/2$–π as they are in the calculation of b_b/b.

Phase functions with lower b_b/b have narrower angular distributions. For multiple collisions the effective angular distribution spreads rapidly. Furthermore, the relative spread

is more rapid for the narrow angular distributions. For instance, an isotropic distribution is unaffected by the number of collisions. Thus, for multiple scattering the differences between the single scattering Phase functions used to describe water type become less important. Statistically, collision broadened angular distribution is very similar to a broader single scattering distribution; both are described by Legendre polynomials in $\cos(\theta)$ where θ is the scattering angle (KORTUM, 1969). In Monte Carlo simulations, the effect of multiple collisions is hidden but it is responsible for the fact that JEROME et al. (1996) were able to fit the proportionality $R_{RSW} \propto Bb/a$ with a single polynomial, a polynomial whose main term in b/a is comparable with $C_b \sim 0.112(B')$, where B' represents the average B. Equation 2, used here, will not give results as accurate as equation 1b, but Equation 2 is simple and it is indispensable in the first order estimate of b without the need for an a-priori guess on the value of b_b/b.

Returning to equation 2, we note that in principle we could simulate R_{RSW} for any coastal water if we knew in advance the spectral dependence and magnitude of a_{DOM}, a_p, a_c, and b precisely. Indeed, this is often done in commercially available simulation programs. Commercial programs predict what R_{RSW} "should be" if we have ground truth measurements of a_{DOM}, a_p, a_c, and b and assume knowledge of b_b/b. However, we wish the converse, i.e. we want to determine the magnitude and the spectral dependence of a_{DOM}, a_p, a_c, and b from the measurement of R_{RSW} alone and subsequently from R_{SR} alone.

At first sight, a multifunctional fit to equation 2 based on the general optical properties of a_{DOM}, a_p, a_c, and b seems feasible and straightforward. However, since R_{RSW} in equation 2 depends only on the ratio b/a, it has several close yet false solutions for multiples common to both b and a. In reality, false solutions are the norm in random multi-parameter fits to R_{RSW} in the visible spectrum. To prevent false solutions we will establish a thumb rule for the relationship between b and a_p at 400 nm. We also set up restrictions on the spectral dependence of optical parameters so the sequential iterative search for solutions to R_{RSW} will be limited to realistic values of the absorption and scattering coefficients.

GENERAL OPTICAL PROPERTIES OF COASTAL WATER

To obtain general characteristics of the constituents of coastal water, we examine the wavelength dependence for b, b_b, a_{DOM}, a_p, and a_c for three geographic regions that provide wide variety of suspended solids and DOM. Other regions such as the coastal waters off North Carolina and the Chesapeake Bay gave similar results. Thus, for the purposes of this study, we assume that coastal waters of Great Bay, NJ, the Mississippi Sound, and the coastal regions of Lake Superior are representative of the coastal waters in general. In short, we deal with coastal waters that are usually composed of wide mixtures of particulate and DOM from large coastal regions. Individual species of phytoplankton (VOLTEN et al., 1998) and mineral particles (DIEHL et al., 1978) do have differing scattering functions. However, broad aggregates of inorganic particles and dissolved organic matter have similar optical properties. This is evident from VOLTEN et al. (1998)
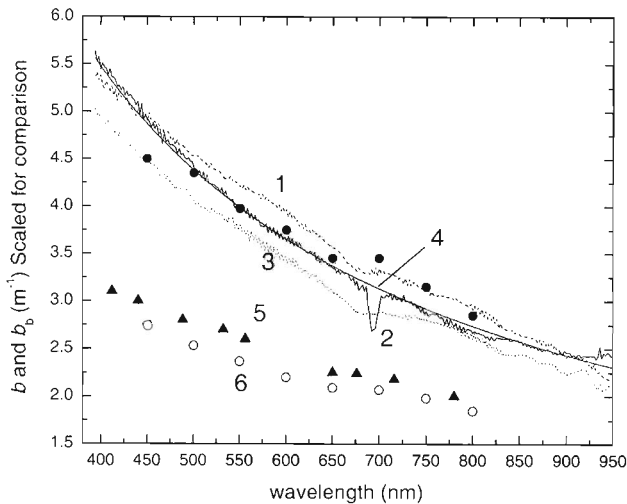
Figure 1. Curves for b, b_b, and b_f in this figure are scaled for the sake of comparing the wavelength dependence of b and b_b. Curves 1 through 4 are all for Allouez Bay, WI. Curve 1 shows $(0.25 \times b)$. Curve 2 shows $(15 \times b_b)$. Curve 3 shows $(2 \times b_f)$ twice the forward scattering at 2–7°. Curve 4 shows $1/\lambda$ fit to Curve 2. Curve 5 shows the experimental points for b for Great Bay, NJ (courtesy Boss E., Pegau S., 2000. LEO 15 data from joint experimental cruise by NRL, Oregon State University, and Rutgers University). Curve 6 shows the experimental points for $(11 \times b_b)$ from Whitlock *et al.* (1981) scaled for comparison with the wavelength dependence shown by Curve 5.
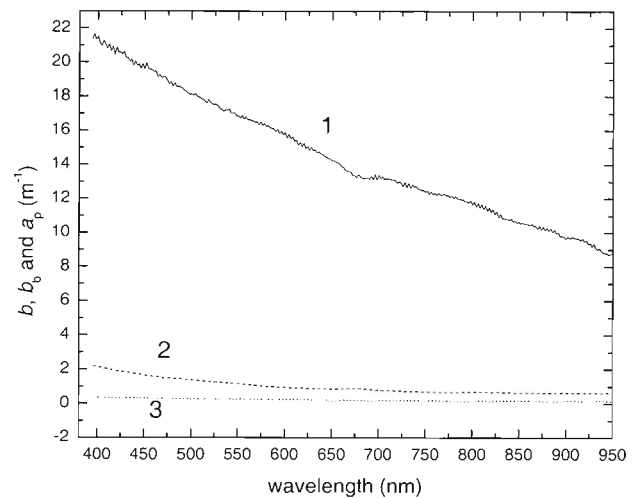

Figure 2. The relative magnitude of b, a_p, and b_b is shown by Curves 1, 2, and 3 respectively, all for Allouez Bay, WI. Note that $b_b/b \sim 0.016$ at $\lambda = 400$ nm, and $a_p/b \sim 0.1$. Such results gave rise to the thumb rule relationship between b, a_p and b_b used in the text.

and Kirk (1994). The data for the three regions used here provides only the general spectral character of b, a_{DOM}, and a_p. By allowing reasonable variation of parameters we hope to encompass most, though not all, other coastal regions. On the other hand, a_c does not have an easily quantifiable global spectral form, but it does have a common spectral signature at ~676 nm (Bricaud *et al.*, 1995). Thus, we can use a surrogate "average" a_c to adjust for the *difference* at 676 nm between the measured R_{RSW} and R_{RSW} simulated using best the estimates of b, a_{DOM}, and a_p.

Wavelength Dependence of $b(\lambda)$ and $b_b(\lambda)$

Typical spectral dependence for b_b and b is shown in Figure 1. The wavelength dependence of b and b_b presented here was based on *in situ* data using standard ac9 meters, and the results published by Whitlock *et al.* (1981); and Sydor and Arnone (1997) supplemented by laboratory measurements that extend the published data beyond 700 nm. We can see from Figure 1 that typical behavior for $b(\lambda)$ follows the $(1/\lambda)^n$ dependence, where $n \sim 1$. In general, we can approximate the overall wavelength dependence of $b(\lambda)$ with:

$$b(\lambda) \sim b_{730}(730/\lambda)^n \qquad (3)$$

where n ranges over the interval $1.2 > n > 0.8$, and b_{730} is a convenient mid-range reference value for b at 730 nm. Figure 1 shows that b_b, and b, and the forward scattering coefficient, b_f, have similar monotonic spectral dependence over the entire 400–900 nm spectral range.

Wavelength Dependence of $a_p(\lambda)$ and the Relative Magnitude of a_p and b

Figure 2 shows the relative magnitudes of b, a_p and b_b. The wavelength dependence of a_p was determined using filter pad analysis with beta factor = $1/(0.258 + 1.153*\text{pad optical density})$. Samples were passed through 25 mm GF/F filters with nominal 0.7 μm sized pores and hot methanol was used to leach out the organic material. Filter pad deposits bleached with methanol provided for a reasonable separation of the wavelength dependence of a_p, and a_c. As a final check, we compared the total absorption from filter pads plus the absorption by DOM filtered through 0.2 μm and 0.7 μm pore filters with the total absorption measured using ac9 meters. The results in Figure 3 and Figure 4 show that a_p has an overall exponential character given by:

$$a_p(\lambda) \sim a_{p400}\exp((400 - \lambda)/L_p) \qquad (4)$$

where a_{p400} is the absorption coefficient due to inorganic matter at 400 nm, and L_p is the mean absorption wavelength for inorganic matter. L_p ranges from 90 to 120 nm. The range of L_p suggests that we should not set a_p to zero at 730 nm for heavily silt laden coastal waters as is often done in calibration of ac9 meters for open ocean applications. Examination of the relative magnitudes of a_p and b for 29 stations provides us with an important *thumb rule*: $a_{p400} \sim (0.1 \pm 0.03)b_{400}$ and $b_b \sim .02b$.

Wavelength Dependence of a_{DOM}

The average wavelength dependence of a_{DOM} was derived from absorption by coastal water passed through 0.2 μm or 0.7 μm pore filters. Figure 5 shows that a_{DOM} has an exponential behavior given by:

$$a_{DOM}(\lambda) = a_{DOM400}\exp((400 - \lambda)/L_D) \qquad (5)$$
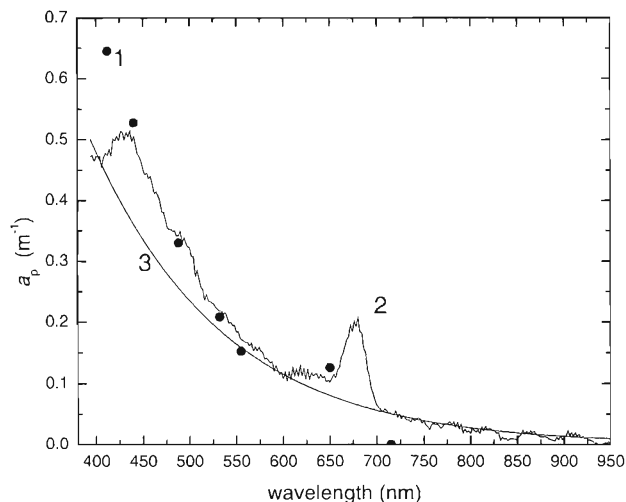
Figure 3.   Wavelength dependence for a_p. Curve 1 shows the experimental points for absorption by suspended particles (organic + inorganic) due to b ~ 3.5 m^{-1} for Great Bay, NJ (courtesy BOSS E., PEGAU S., 2000. LEO 15 data from joint experimental cruise by NRL, Oregon State University, and Rutgers University). Curve 2, jagged solid line, shows filter pad data for absorption by suspended solids (organic + inorganic) for Minnesota Shore of Lake Superior (2 mg/l suspended solids). Curve 3, smooth solid line, shows a_p for filter pad (Curve 2) bleached with hot methanol.

Again, a_{DOM400} is the reference absorption coefficient for DOM at 400 nm and L_D is the mean absorption wavelength for DOM. Note L_D has 55–70 nm range, roughly a factor of two shorter than L_p.

Absorption by Pure Water a_w

Published tables for a_w due to pure water and clear ocean water differ in the ~730 nm region of the spectrum. We used our own laboratory measurements of a_w for pure water adjusted to the published values for a_w at 700, 800 and 900 nm [SMITH and BAKER, 1981; POPE and FRY, 1997; CURCIO and PETTY, 1951; and KUO et al., 1993].

Absorption by Chlorophyll

Chlorophyll is found in living matter. Figure 6 shows that the spectral distribution of $a_c(\lambda)$ varies widely even in one geographic locality. The absorption peak at 676 nm in Figure 6 is the most distinctive chlorophyll feature in R_{RSW} (BRICAUD et al., 1995). This feature can be quantified in derivatives of smoothed R_{RSW} spectra ($dR_{RSW}/d\lambda$). However, the correlation of a_c at 676 nm with total chlorophyll concentration was poor. For 10 stations in St. Louis Bay, MS, we obtained correlation coefficient $r^2 = 0.64$ (SYDOR et al., 1997). We use filter pad measurements of $a_c(\lambda)$ for clear waters of Lake Superior (10 m Secchi transparency) as a representative surrogate shape for a_c used in adjusting the final magnitude of simulated R_{RSW} at 676 nm. Since chlorophyll concentration in the barren cold waters of Lake Superior is low, we multiply its a_c by a factor of 5 to obtain the surrogate "average a_c" shown in Figure 6. The choice of Lake Superior a_c is strictly intuitive (in retro-
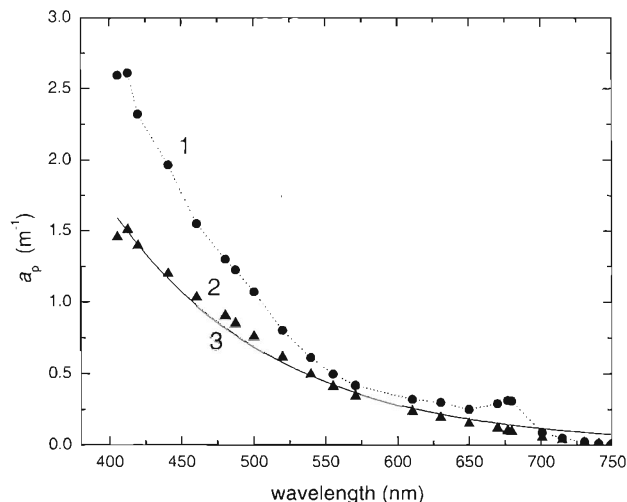

Figure 4.   Curve 1, solid circles with dotted line, show the filter pad absorption from suspended solids (organic + inorganic) for b ~ 8 m^{-1} in for St. Louis Bay, MS. Curve 2, up triangles, show a_p for inorganic solids from the filter pad bleached with hot methanol. Curve 3, smooth solid line, shows an exponential fit to the up triangles yielding $L_p = 112$ nm.

spect we could have used BRICAUD et al. 1995 average a_c). Aside from the fact that we know Lake Superior, we observed that a_c for Lake Superior had low values at ~400 nm. Thus, by using Lake Superior a_c to adjust the final magnitude of the simulated R_{RSW} at 676 nm, we did not destroy the prior fit of R_{RSW} due to a_{DOM} and a_p at 400 nm. As a result, we did not have to deal with backed out a_c that had negative values at 400 nm in comparison with the surrogate a_c.
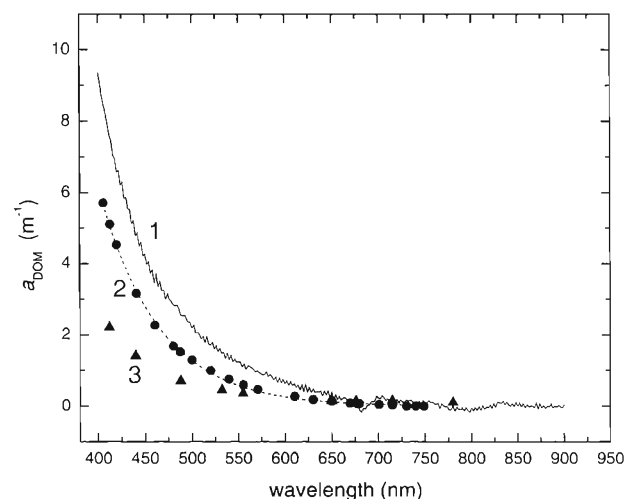

Figure 5.   General wavelength dependence of a_{DOM}. Curve 1 shows the absorption by DOM for Allouez Bay, WI. Curve 2, solid circles, show the absorption by DOM in St. Louis Bay, MS. The dashed line through the solid circles yields $L_d = 63$ nm. For comparison, Curve 3, up triangles, show a very similar wavelength dependence for a_{DOM} in Great Bay, NJ (courtesy BOSS E., PEGAU S., 2000. LEO 15 data from joint experimental cruise by NRL, Oregon State University, and Rutgers University).
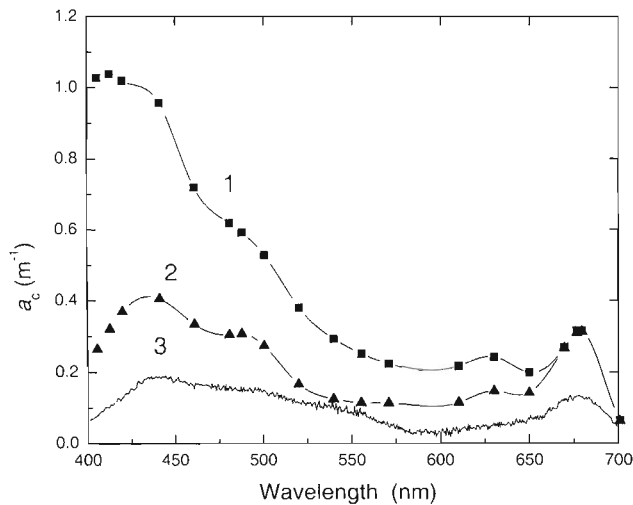
Figure 6. Phytoplankton pigment does not have a readily quantifiable spectral shape. a_c is usually determined from the difference in the transmission by bleached and unbleached filter pads. Curves 1 and 2 show two nearby stations in St. Louis Bay, MS. Curve 3 shows (5 × a_c) for Lake Superior (10 m Secchi transparency). We chose Curve 3 as the representative "average" shape for a_c.
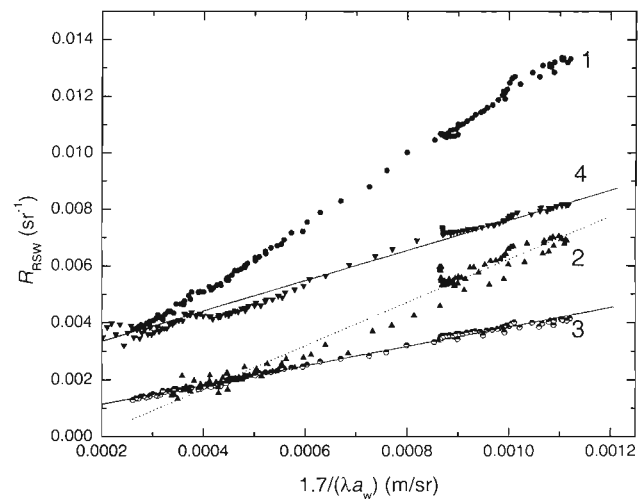

Figure 7. Plots of R_{RSW} vs. $1.7/(\lambda a_w)$ fall along straight lines. Slopes of the lines give the initial estimates of b_{730} based on C_b = .0023 in the 750 < λ < 930 nm region of the spectrum. Curve 1 is for Allouez Bay, WI, yielding $b_{730} \sim 10$ m^{-1}. Curve 2, triangles with the best line fit, is for St Louis Bay, MS, with $b_{730} \sim 7$ m^{-1}. Curve 3, half circles, is for Duluth Harbor, MN, yielding $b_{730} \sim 3.2$ m^{-1}. Curve 4, down triangles with best line fit, is for Great Bay, NJ, for $b_{730} \sim 5.6$ m^{-1}.

Infrared Properties of Bulk Reflectance

It has been our experience (SYDOR and ARNONE, 1997) that R_{RSW} is directly proportional to $b_{730}/(\lambda a_w)$ for λ > 750 nm as shown in Figure 7. For instruments with steady dark current and good signal to noise ratio, plots of R_{RSW} vs. $1/(\lambda a_w)$ for 750 < λ < 900 nm yield straight lines passing close to the origin. We will use the slope of R_{RSW} vs. $1.7/(\lambda a_w)$ to obtain the initial estimate of the magnitude of b_{730}. The factor 1.7 comes from taking b_{730} as the reference value for b in Equation 3, taking n = 1, and taking C_b = 0.0023. This value of C_b is roughly compatible with f/Q $\sim$ 0.1, and $b_b/b \sim$ 0.02. For instance, MOREL and PRIEUR (1977) give E_u^-/E_d^- = .33b_b/a. If we take Q $\sim \pi$ (see for example GONS, 1999), then $R_{RSW} \sim L_u^-/E_d^- \sim$ (0.11)b_b/a. This leads to $R_{RSW} \sim$ (0.11)(.02)b/a , or $R_{RSW} \sim$ 0.0022b/a, reasonably close to our experimental value C_b = 0.0023. This value of C_b is also borne out by the main term in JEROME et al. (1996). Their average value of B excluding the extreme values is 0.024, and the coefficient in front of the term in Bb/a is 0.112, leading to $C_b \sim$ 0.0027. JEROME's negative third term brings the result even closer to 0.0023. However, their polynomial fit should not have included a constant since in principle R_{RSW} should go to zero for b = 0, and should never be negative.

Measurement of $R_{RSW}(\lambda)$

We measured R_{RSW} using a calibrated submersible reference target and a submersible probe coupled to a field spectrometer. Both L_u and E_d^- were measured $\sim$10 cm below the water surface under calm conditions. Judging from repetitive scans, the accuracy of R_{RSW} was $\sim$5%. However, the total accuracy of the in-water measurement for b(λ), a(λ), and $R_{RSW}(\lambda)$ was no better than 10%. We found that average value

of $C_b \sim$ .0023 sr^{-1} used originally for Lake Superior worked well in other waters. As a result, we use this value of C_b to estimate b_{730} for all three geographic regions. We did so in spite of the fact that measurements of b_b/b differed for the three regions. We wanted to establish a general spectroscopic method rather than one that was site specific.

MULTI-PARAMETER FITTING PROCEDURE

Determination of the Initial Values of b_{730}, a_{p400}, and a_{DOM400}

We obtained the starting value for b_{730} from the slope of R_{RSW} vs. $1.7/(\lambda a_w)$ for 750 < λ < 900 nm, as shown in Figure 7. Subsequently, we estimated b(λ) using equation 3. Then, we took a_{p400} = 0.1 b_{400} according to the thumb rule and used L_p = 110 nm in equation 4 to estimate the initial $a_p(\lambda)$. We estimated a_{DOM400} by solving Equation 2 at 400 nm using the initial values of a_{p400} and b_{400}. We assumed L_D = 60 nm to obtain the initial $a_{DOM}(\lambda)$ from Equation 5.

Fitting Procedure and Examples of the Results

We start the simulation of R_{RSW} using the initial estimates of b(λ), $a_p(\lambda)$, and $a_{DOM}(\lambda)$ and a_c = 0 in Equation 2 and examine the first approximation for λ > 750 nm. We adjust b_{730} and n within the above prescribed limits to obtain a close fit between the simulated and measured $R_{RSW}(\lambda)$ in the 750–900 nm region of the spectrum. This procedure is tantamount to adjusting the *product* C_bb, thus subsequent correction of R_{RSW} for the absorption in the visible region of the spectrum is independent of the estimate of b based on C_b = 0.0023.

It is very important in the first simulation to examine the position of R_{RSW} peak at $\sim$800 nm, (see Figures 8–11). This
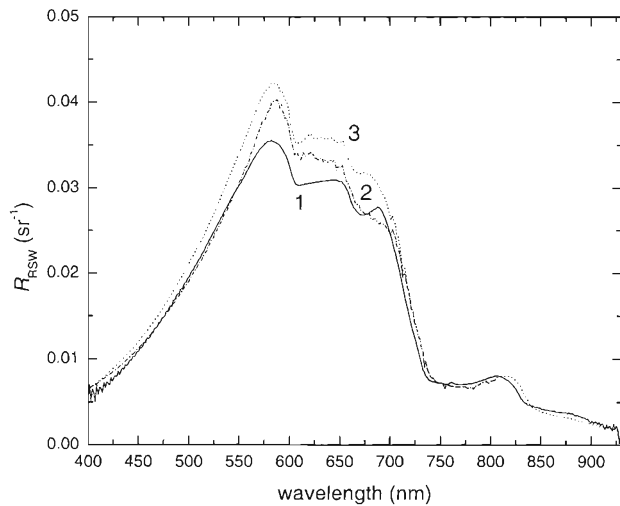
Figure 8. Curve 1 shows measured R_{RSW} for Great Bay, NJ. Curve 2 shows the simulated R_{RSW} using the best values of b, a_{DOM}, a_p, and "average" a_c. Curve 3 shows the simulated R_{RSW} setting $a_c = 0$. The difference between Curve 3 and Curve 1 yields $a_c(\lambda)$ shown by Curve 2 in Figure 12.
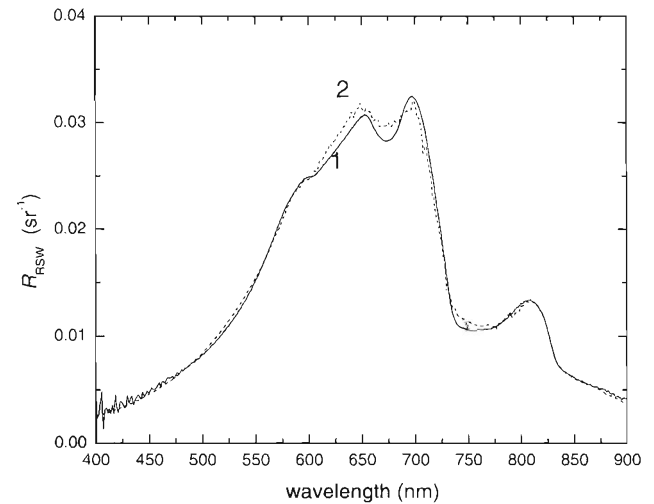

Figure 10. High DOM and high particle concentration in Allouez Bay, WI, shows observed $R_{RSW}(\lambda)$, Curve 1, similar to the one shown in Figure 9, except the magnitude of R_{RSW} is much higher in Allouez Bay because of high suspended load ($\sim$ 30 mg/l). In the simulation shown by Curve 2 we observe again a close reproduction of the fine features of the measured R_{RSW} shown by Curve 1.

peak corresponds to a structure in a_w. If the wavelength calibration of the field spectrometer is off, the peak at ~800 nm will not coincide in the simulated and measured spectrum. Furthermore R_{RSW} vs. $1.7/(\lambda a_w)$ exhibited in Figure 7 would not have formed a straight line.

Having obtained the best fit to R_{RSW} in the 750–900 nm region of the spectrum, we adjust a_{p400} to the newly obtained $C_b b$. We then readjust a_{DOM400} to acquire coincidence between the simulated and measured R_{RSW} at 400 nm. Subsequently, we go through an iteration routine using small variations in
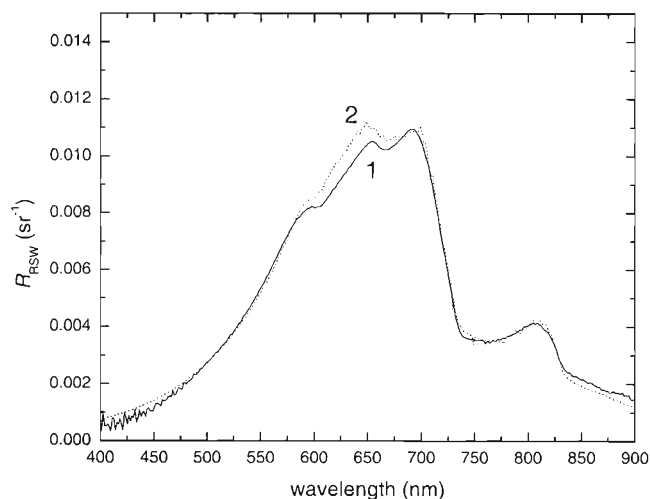

Figure 9. High a_{DOM} but low a_c in Duluth Harbor, MN, exhibits simulated R_{RSW}, Curve 2, that reproduces faithfully nearly all the fine features of the observed R_{RSW} shown by Curve 1. This result supports the use of the spectral shape of $b(\lambda)$ in place of $b_b(\lambda)$ in equation 1a.
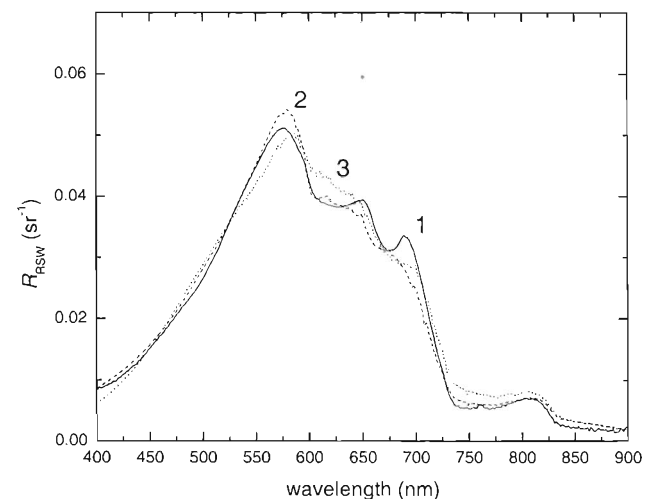

Figure 11. Simulation of R_{RSW} must follow the sequenced curve fitting procedure and parameter restrictions. Here we see a simulation of R_{RSW} for St. Louis Bay, MS. The solid Curve 1 shows measured R_{RSW} due to $a_{412} = 3.02$ m^{-1}, $b_{412} = 10.1$ m^{-1}, and average $a_c \sim 0.4$ m^{-1}. Curve 2 shows the systematic simulation of R_{RSW} yielding predicted $a_{412} = 3.1$ m^{-1}, $b_{412} = 11.4$ m^{-1}, and average $a_c = 0.35$ m^{-1}. On the other hand an *unrestricted iterative fit* to R_{RSW} produces a close solution shown by the dotted Curve 3. The unrestricted solution yields an order of magnitude larger a and b over the visible spectrum, giving $a_{412} = 17.2$ m^{-1}, $b_{412} = 58.5$ m^{-1} and average $a_c = 0.25$ m^{-1}. Comparison of a and b due to measured, restricted, and unrestricted simulation of R_{RSW} is shown in Figure 13.
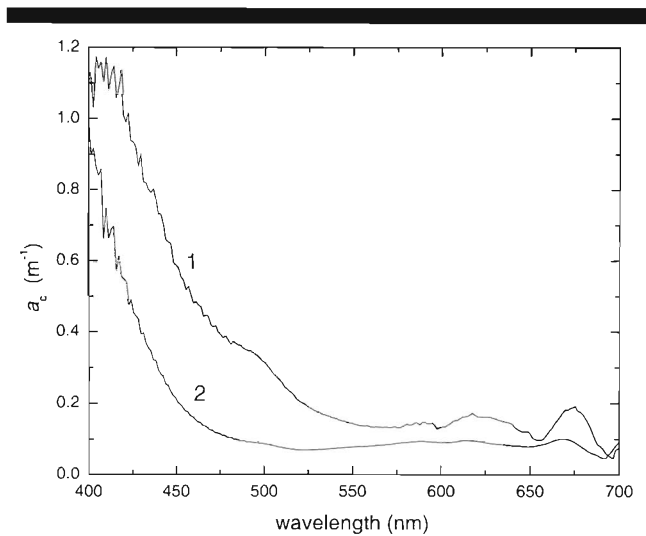
Figure 12. Curve 1 shows a_c determined from R_{RSW} exhibited by Curve 1 in Figure 11. Compare this a_c with filter pad data shown by Curve 1 in Figure 6. Curve 2 in this figure shows chlorophyll absorption for Great Bay, NJ derived from R_{RSW} shown in Figure 8. Measurement of a_c was unavailable at this station but the value and shape of the predicted a_c shown by Curve 2 is comparable with measured a_c in the same geographic region.
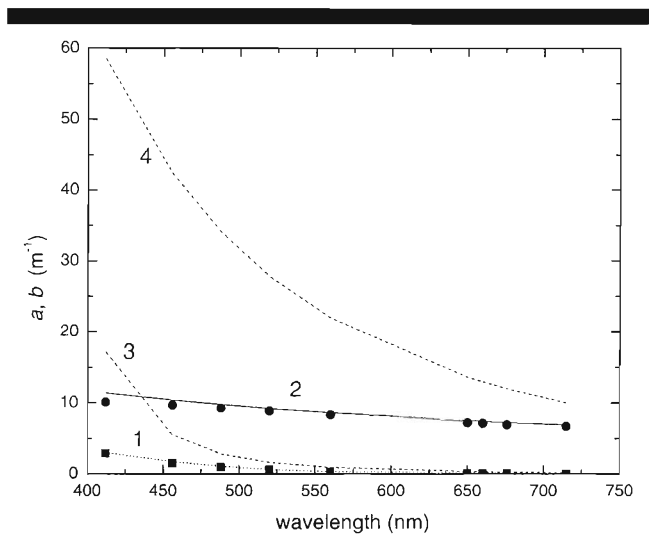

Figure 13. Systematic fit to R_{RSW} in Figure 11 yields a and b shown by the dotted and solid lines Curve 1 and 2 respectively. Corresponding ac9 values of a and b are shown by the discrete points. Dashed lines, Curves 3 and 4 show a and b resulting from an unrestricted iterative fit to R_{RSW}. Since the false fit shown by Curve 3 in Figure 11 is close to the actual R_{RSW} in the visible spectrum, visible band ratios could hardly predict correct a_{DOM}, b, and a_c unless some site specific limits were imposed on the magnitudes of b and a_{DOM}.

a_{p400}, a_{DOM400}, L_p and L_D to obtain a close fit to R_{RSW} over the 400–600 nm region of the spectrum.

Having obtained a good fit for both the 400–600 nm and the 750–900 nm ends of the spectrum, we add 0.2–1.5 multiples of the "average" a_c in equation 2 until we obtain the same amplitude for the simulated and measured R_{RSW} at 676 nm. This last procedure upsets slightly the previously close fit in the 400–600 nm region. We readjust a_p and a_{DOM} to again obtain a close fit in the 400–550 nm region but the simulated R_{RSW} with "average" a_c added should still coincide with the measured R_{RSW} at 676 nm. If the absorption by pigment is less than 0.1a at 600 nm, the final simulation of R_{RSW} is usually very close to the measured R_{RSW} at both ends of the spectrum and at 676 nm, as shown in Figures 8–11. If a_c < .05a at 600 nm, the fit will be close over the entire 500–700 nm region, as seen in Figure 9 and Figure 10.

To determine the true a_c, we assume that the difference between measured R_{RSW} and R_{RSW} simulated using the best values of $C_b b(\lambda)$, $a_p(\lambda)$ $a_{DOM}(\lambda)$ and a_c = 0, is due to the true shape of a_c. To determine actual a_c, we solve:

$$a_c = (C_b b/R_{RSW}) - a_{T0} \qquad (6)$$

R_{RSW} in Equation 6 is the measured bulk reflectance, a_{T0} is the estimated total absorption coefficient obtained for the sum of a_{DOM}, a_p, and a_w used in the best fit. An example of the predicted a_c is shown in Figure 12.

Demonstration of a False Fit

We emphasized that it was important to follow a systematic approach to the multi-parameter simulation of R_{RSW}. We demonstrate this using the data in Figure 11. The station for which R_{RSW} is shown in Figure 11 had a measured average

$a_c \sim .4$ m^{-1}, as shown by Curve 1 in Figure 6. The corresponding value of a and b for the station are shown by the discrete points in Figure 13. Using an unrestricted iterative fit to R_{RSW}, we obtained a variety of close solutions that gave a and b roughly five times larger than the measured values. Notice that b/a is nearly the same for the real and false cases, as was expected from Equation 1b, and Equation 2. The unrestricted fit to R_{RSW} is shown in Figure 11 by Curve 3. Curve 2 in Figure 11 shows the systematic fit to R_{RSW}. The systematic fit produces reasonable estimate of a_c as shown by Curve 1 in Figure 12 in comparison with Curve 1 in Figure 6. The systematic fit also produced accurate estimates of a and b, as shown in Figure 13. Since the systematic and false fits had comparable r^2 correlation coefficients, the unrestricted fit demonstrates that there are many close yet false solutions in the visible spectrum. This is also the reason why band-ratio algorithms performed in the visible spectrum are site-specific and often fail in global predictions of a_c, b, and a_{DOM}.

In summary, the selection of true solution to R_{RSW} depends on the setting of limits on L_D, L_p, and n, and applying the fit sequentially in the four regions of the spectrum where we can link R_{RSW} to the general optical properties of the constituents. When we follow the prescribed routine, the values for the absorption and scattering coefficients agree quite closely with in-water ac9 data, as demonstrated for Lake Superior in Figure 14.

The actual fitting routine can be programmed using Microcal Origin or an equivalent software package.

CONCLUSION

We presented a procedure for fitting the diffuse reflectance spectra from coastal water by identifying the spectral regions
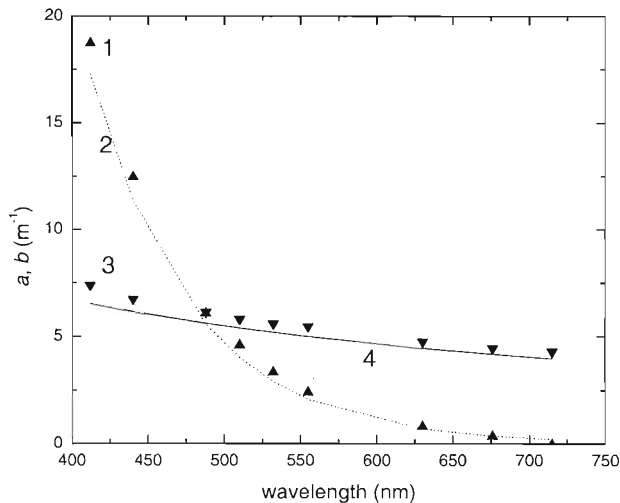
Figure 14. This figure shows another example of the closeness of predicted and measured a and b resulting from a systematic fit to R_{RSW} for Duluth Harbor, MN. ac9 values of a are shown by the up triangles, labeled with numeral 1. The dotted line, Curve 2, shows a derived from the systematic simulation of R_{RSW} shown in Figure 9. Down triangles labeled with numeral 3, show ac9 values of b in comparison with the predicted $b(\lambda)$ shown by the solid line, Curve 4.

where R_{RSW} can be linked to individual optical parameters. The *in situ* data and laboratory measurements were used only to determine the spectral character of the optical parameters in coastal water. The data presented here was not meant and is not a definitive study of the three regions used in this presentation. We provided a range for optical parameters to make the technique applicable globally, but it is certainly not all-inclusive.

We show that measurement of R_{RSW} in the 750–900 nm region of the spectrum is critical because its spectral shape in that region depends mainly on a_w and b. Slope of R_{RSW} vs. (λa_w) in the near infrared determines the product $C_b b$. By assuming that C_b is flat and has a global value, we can estimate b for an unknown station. The estimate of b depends on the variability of C_b. In the regions considered here the accuracy for b is $\pm 15\%$. It is important to note that determination of the sum of a_p, a_{DOM}, and a_c does not depend on the accuracy of the estimated b. Estimates of total a depend on the ratio of R_{RSW} in visible and near IR, independent of $C_b b$. Therefore, $a(\lambda)$ is determined *relative* to known a_w in the 750–900 nm region of the spectrum. The error in estimated a depends only on the accuracy of R_{RSW}.

The thumb rule allows for a rough division the total absorption into a_p and a_{DOM} in the ~600 nm region of the spectrum where a_w is often relatively small for coastal waters. If the concentration of phytoplankton pigment is relatively low, the absorption in the 400 nm region of the spectrum is often dominated by a_{DOM}. Otherwise, a_{DOM} competes with a_c. However, a_{DOM} is monotonic, unlike a_c, thus we can pick off the structure in R_{RSW} at 676 nm and link it to a_c at 676 nm.

We relied on the use of $b(\lambda)$ rather than $b_b(\lambda)$. Our argument why this is fundamentally correct is based on consid-

erations of multiple scattering and the fact that b and b_b appear to have similar spectral dependence. If equation 2 was not valid and the spectral dependence of b was markedly different from b_b, we should not have observed a direct proportionality between R_{RSW} and b/a_w for 750 < λ < 900 nm. We observed a linear relationship in an overwhelming number of cases, yielding similar value of C_b. Furthermore, if our assumption of equation 2 was wrong and our characterization of the optical parameters was incorrect, we would be unable to reproduce the fine spectral features in R_{RSW} shown in Figure 9 and Figure 10.

By using b rather than b_b we might conjecture that the greatest source of error in the estimates of b_{730} from R_{RSW} vs. $1.7/(\lambda a_w)$ come from the variability of b_b/b. For Coastal Waters, b_b/b ranges from 1.3% to 4.4%, roughly a factor of three (JEROME *et al.,* 1996). Thus, our taking C_b ~ 0.0023 as a constant should produce an error of at least 100% in the estimates of b_{730}. Normally, our estimate of b was far more accurate. Instead, the greatest source of error appeared to come from the changing light conditions during the measurement of R_{RSW} on partly cloudy days.

Laboratory measurements indicate that we can extend ac9 measurements of the wavelength dependence of b to wavelengths longer than 700 nm. Our measurements of the wavelength dependence of b_b at 175° and b_f at 5° agree with the wavelength dependence of b and b_b presented by WHITLOCK *et al.* (1981).

Carefully restricted multi-parameter fits to R_{RSW} can yield the magnitude and the wavelength dependence of $a_{DOM}(\lambda)$ and $a_p(\lambda)$ to an accuracy of 15% for waters where inorganic particles or DOM dominate a *i.e.* where a_c < 0.1a at 600 nm. At this stage, our determination of $a_c(\lambda)$ is tenuous because of the great variability of a_c at 400 nm where it often competes with the magnitude of a_{DOM400}. A reliable method for separating a_c from a_{DOM} at 400 nm is needed for more accurate estimates of $a_c(\lambda)$ from multi parameter fits to R_{RSW}.

ACKNOWLEDGEMENTS

LITERATURE CITED

BRICAUD, A.; BABIN, M.; MOREL, A., and CLAUSTRE, H., 1995. Variability in chlorophyll-specific coefficients of natural phytoplankton. *Journal of Geophysical Research,* 100, 13321–13332.

CURCIO, J. A. and PETTY, C. C., 1951. The near infrared absorption spectrum of liquid water. *Journal of the Optical Society of America,* 41(5), 302–304.

DIEHL, S. R.; SMITH, D. T., and SYDOR, M., 1979. Analysis of suspended solids by single-particle scattering. *Applied Optics,* 18, 1653–1658.

GONS, J. H., 1999. Optical teledetection of chlorophyll a in turbid inland waters. *Environmental Science and Technology,* 33, 1127–1132.

GORDON, H. R.; BROWN, O. B., and JACOBS, M. M., 1975. Computed relationship between the inherent and apparent optical properties of a flat homogenous ocean. *Applied Optics,* 14, 417–427.

JEROME, J. H.; BUKATA, R. P., and MILLER, J. R., 1996. Remote sensing and its relationship to optical properties on natural waters. *International Journal of Remote Sensing,* 17, 3135–3155.

KIRK, T. O., 1994. Characteristics of the light field in highly turbid waters, a Monte Carlo study. *Limnology and Oceanography,* 39, 702–706.

KORTUM, G. 1969. *Reflectance Spectroscopy.* New York: Springer Verlag, pp. 90–110.

KUO, L.; LABRIE, D., and CHYLEK, P., 1993. Refractive indices of water and ice in the 0.65–2.5 μm spectral range. *Applied Optics,* 32, 3531–3540.

MOREL, A.; VOSS, J. V., and GENTILLI, B., 1995. Bidirectional reflectance of oceanic water: a comparison of modeled and measured upward radiance. *Journal of Geophysical Research,* 100(13), 143–151.

MOREL, A. and PRIEUR, L., 1977. Analysis of variations in ocean color. *Limnology and Oceanography,* 22, 709–722.

PETZOLD, T. J., 1972. *Volume Scattering Function for Select Ocean Waters.* University of California, San Diego, Scripps Institute of Oceanography Visibility Laboratory. SIO Ref. 72-28.

POPE, R. M. and FRY, E. S., 1997. Absorption spectrum (380–700 nm) of pure water. *Applied Optics,* 36(33), 8710–8723.

SMITH, R. C. and BAKER, K., 1981. Optical properties of the clearest natural waters. *Applied Optics,* 20, 177–184.

SYDOR, M. and ARNONE, R. A., 1997. Effect of suspended particulate and dissolved organic matter on remote sensing of coastal and riverine waters. *Applied Optics,* 36, 6905–6912.

SYDOR, M.; ARNONE, R. A., and GOULD, R. A. Jr., 1997. Remote sensing of case 2 waters. *Ocean Optics* XIII Proceedings of SPIE, 2963, 222–227.

SYDOR, M.; ARNONE, R. A.; GOULD, R. W., JR.; TERRIE, G. E.; LADNER, S. H., and WOOD, C. G., 1998. A new remote sensing technique for determination of the volume absorption coefficient of turbid water. *Applied Optics,* 37, 4944–4950.

VOLTEN, H.; DE HAAN, J. F.; HOVENIER, J. W.; SCHREURS, R.; DEKKER, A. G.; HOOGENBOOM, H. J.; CHARLTON, F., and WOUTS, R., 1998. Laboratory measurements of angular distribution of light scattered by phytoplankton and silt. *Limnology and Oceanography,* 43, 1180–1197.

WHITLOCK, C. H.; POOLE, L. R.; USRY, J. W.; HOUGHTON, W. M.; WITTE, W. G.; MORRIS, W. D., and GURGANUS, E. A., 1981. Comparison of reflectance with backscatter and absorption parameters for turbid water. *Applied Optics,* 20, 517–522.